AIP | Journal of Applied Physics

Tip size effects on atomic force microscopy nanoindentation of a gold single crystal

Marcel Lucas, Ken Gall, and Elisa Riedo

Citation: J. Appl. Phys. **104**, 113515 (2008); doi: 10.1063/1.3039511
View online: http://dx.doi.org/10.1063/1.3039511
View Table of Contents: http://jap.aip.org/resource/1/JAPIAU/v104/i11
Published by the American Institute of Physics.

Tip size effects on atomic force microscopy nanoindentation of a gold single crystal

Marcel Lucas,[1] Ken Gall,[2] and Elisa Riedo[1,a)]
[1]*School of Physics, Georgia Institute of Technology, Atlanta, Georgia 30332-0430, USA*
[2]*School of Materials Science and Engineering and George Woodruff School of Mechanical Engineering, Georgia Institute of Technology, Atlanta, Georgia 30332-0245, USA*

(Received 8 August 2008; accepted 23 October 2008; published online 8 December 2008)

The effect of tip radius on atomic force microscopy (AFM) nanoindentation is investigated through indentation on the (111) face of a gold single crystal. The hardness is derived using two different methods: by measuring directly the projected area of the residual indent with AFM images and by measuring the cross-sectional area of the indenter before and after each nanoindentation test. The hardness values obtained from the cross-sectional area of the indenter are comparable with those obtained from images of the residual indent scanned with a sharp tip. Two AFM tips of average radii of 70 ± 12 and 112 ± 26 nm are used to indent the sample to various depths ranging from 4 to 50 nm. For depths above 30 nm, hardness values remain constant around 500 MPa for both indenters. For depths below 30 nm, the hardness increases as the indent depth decreases for the sharp and blunt indenters, and the indent depth dependence is observed over a wider depth range for the sharp indenter. For depths below 30 nm, the hardness values obtained with the sharp indenter are also consistently higher than those obtained with the blunt indenter. The results confirm a size scale effect during nanometer scale indentation for both varying penetration depth and tip radius, both of which influence the volume of material sampled during deformation. © *2008 American Institute of Physics*. [DOI: 10.1063/1.3039511]

I. INTRODUCTION

Microindentation has been widely used to study the mechanical properties of a material and represents an alternative to tensile testing for nanostructures, brittle materials, or thin films.[1,2] Technical advances in the past decade even enabled nanoindentation measurements. The popularity of the technique has increased significantly since new methods have been introduced to determine the hardness and the elastic modulus without the need to image the residual indent.[3,4] The hardness and the elastic modulus are derived from the unloading force-depth curve, which can be analyzed using the relations between the contact stiffness, the contact area, and the reduced elastic modulus, derived by Sneddon for axisymmetric indenters.[5] The method relies heavily on the knowledge of the area function of the indenter, defined as the cross-sectional area of the indenter as a function of the distance from its apex.[3,6] A typical calibration procedure involves indenting a reference material of known elastic modulus and Poisson's ratio, such as fused silica, and measuring the instrument compliance at various depths. The data are then fitted to an area function, assuming, for example, that the indenter is an ideal three-sided pyramid in the case of the Berkovich indenter. The determination of the area function and the contact stiffness requires the introduction of empirical parameters and correction factors, which depend on the indenter shape,[1,7,8] indent depth,[8] and also the material.[2] The accuracy of the area function is especially critical for indentations at maximum depths below 50 nm since even a diamond indenter can experience wear with repeated use at this scale. The apex of the indenter is usually modeled as a sphere, cone, or three-sided pyramid since an accurate measurement of the area function at the nanometer scale is not available on most commercial nanoindentation systems due to the poor lateral spatial resolution and the shape of the commonly used Berkovich indenter.

There has been an intensive effort to model and study experimentally the effect of the tip geometry[7–12] and bluntness[13–17] on hardness values. A greater understanding of the effect of tip shape on hardness will give an insight into the indentation size effect on hardness measurements.[18–21] It has been widely accepted that the indentation size effect has an underlying physical origin, but its interpretation is sometimes debated. For thin films deposited on a substrate, the indentation size effect can be explained by the influence of the substrate, constraint from film thickness, or strain gradient plasticity.[13,22–24] For materials that deform through the motion of dislocations, strain gradient plasticity predicts an indentation size effect driven by geometrically necessary dislocations.[25]

The contribution of tip shape effects to indentation size effects remains uncharacterized and unclear.[18] For example, due to its geometric similarity, a perfectly sharp conical indenter on a homogeneous material would not be expected to cause a size scale effect.[13] However, various hardness measurements on fused silica, which have indicated little depth dependence for a Berkovich indenter,[16] and an increase in hardness with increasing depth for depths below 200 nm for a pyramidal tip sharper than the Berkovich tip,[9] indicate that the magnitude of the indentation size effect depends on the

a)Author to whom correspondence should be addressed. Electronic mail: elisa.riedo@physics.gatech.edu.

indenter shape and possibly on the calibration procedure. Finite element simulations revealed no indentation size effect for ideal conical indenters. However, an indentation size effect is predicted for blunted conical indenters, especially for indent depths smaller than the tip radius.[13] The hardness values were also found higher for conical indenters with a smaller cone angle.[9,18] Earlier work by Tabor[26] on copper with a spherical indenter of 10 mm diameter showed that the hardness increases with the chordal diameter of the indentation. For spherical indenters, it was suggested that the hardness depends on the indenter radius rather than on the indent depth,[17,19] although the smallest indenter radius studied was 14 μm, much larger than the radius of atomic force microscopy (AFM) tips. Finite element simulations showed that for spherical indenters with radii in the nanometer scale, the hardness increases with the ratio of the contact to tip radius.[13,14]

Understanding the effects of the indenter shape on hardness measurements opens the possibility to more directly compare data obtained with different indenters. Most of the hardness data in the literature are currently collected using Berkovich indenters. However, sharper indenters are better suited for the study of hard thin films and thin films of only a few nanometers, where plastic deformation should be constrained to a very small volume.[9,13]

Indenter tip shape can be determined using scanning electron microscopy[27] or transmission electron microscopy,[4] but these techniques are impractical to monitor the tip wear after indentation tests. Alternatively, AFM offers the ability to measure forces in the subnanonewton range and topography with excellent normal and lateral spatial resolution. AFM also enables the direct imaging of the indenter and the accurate determination of the area function around the tip apex.[18,27]

In this study, the hardness of a [111] oriented gold single crystal is measured at depths smaller than 40 nm by AFM. The hardness is measured using two different methods: by measuring the area of the residual indent with AFM images and by measuring the cross-sectional area of the indenter before and after each nanoindentation test. The hardness values obtained with the two methods are compared and the effect of tip radius in AFM nanoindentation is investigated.

II. EXPERIMENTAL

The gold single crystal (99.99% purity, Monocrystals Co., Medina, OH) is oriented in the [111] direction and is 2 mm thick. The nanoindentation force-depth data were collected using a Veeco CP-II AFM with a noncoated silicon tip (NCHR, NanoWorld) or a diamond-coated silicon tip (DT-NCHR, NanoWorld) at room temperature and in air. The DT-NCHR tip is an NCHR tip coated with a 10 nm thick diamond film, so the two tips, which are three-sided pyramids, should have the same face angles. The normal cantilever spring constant was calibrated using the method of Sader *et al.*,[28] 32.2 N/m for the noncoated silicon tip and 44.2 N/m for the diamond-coated tip. The normal force was calibrated by recording the deflection of the cantilever as a function of the scanner displacement while in contact with the silicon substrate. For each nanoindentation test, a new location on the sample was selected, a scanner displacement was chosen, and the duration of the test was set so that the scanner velocity in the normal direction was kept constant at 0.6 μm/s. The indent depth is obtained by subtracting the cantilever bending from the scanner displacement. The adhesion forces were negligible compared to the force required to deform the gold crystal plastically, and thus the contact point can be defined as the scanner position at which the force was minimum. This definition of the contact point reduces the error on the indent depth below 1 nm.

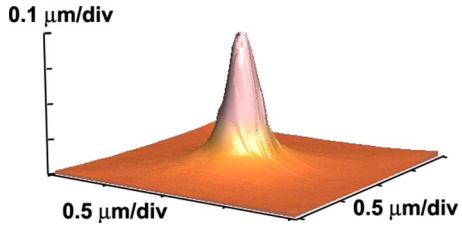

FIG. 1. (Color online) AFM image of the TGT01 silicon calibration grating (MikroMasch, Tallinn, Estonia) collected with a diamond-coated silicon tip.

The hardness was determined using two different methods. In the first one, the hardness is given by the ratio between the maximum load and the area of the residual indent. In the second one, the hardness is defined as the ratio between the maximum load and the cross-sectional area of the indenter at maximum indent depth. For the first method, only the diamond-coated silicon tip was used to indent the gold crystal. The gold crystal was indented three times at various depths and the residual indents were imaged immediately after each indentation using the same diamond-coated silicon tip in tapping mode. After the third indent, the diamond-coated silicon tip was replaced by a new and sharp silicon tip (PPP-CONT, NanoWorld) of tip radius around 10 nm, and the same three indents were scanned again using the sharp silicon tip in contact mode. The area of the residual indent was measured using a flooding method (SPIP software, Image Metrology A/S, Denmark) that identifies all the image pixels below the height of the undeformed sections of the gold crystal.

For the second method, the indenter shape was determined before and after each indentation test by scanning a silicon calibration grating TGT01 (MikroMasch, Tallinn, Estonia), which consists of arrays of inverted silicon tips of heights exceeding 400 nm and with radii smaller than 10 nm. Scanning the grating results in an inverted image of the indenter (Fig. 1). Computational erosion of the image was also used to generate the tip shape, using a blind tip reconstruction algorithm available on the SPIP software.[29] The surface of the tip was generated over an area of 627×627 nm^2 size (81 points $\times$ 81 points). Once the surface of the tip is reconstructed, the cross-sectional area A of the indenter was determined as a function of the distance to the tip apex d by counting the number of image pixels that are below a specified distance from the apex. The difference between the cross-sectional areas obtained with or without computational erosion is smaller than 1%. To monitor the effect of scanning size and scanning velocity on the measured cross-sectional

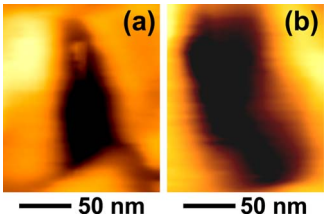

FIG. 2. (Color online) AFM images (150×180 nm^2) of the same indent collected with (a) the indenter and (b) a sharp silicon tip.

areas, 1×1 and 2×2 μm^2 images were scanned at various velocities between 2 and 8 μm/s, but no significant discrepancy was observed in this range.[27]

The area function $A(d)$ was fitted for d ranging from 0 to 40 nm using the model of a perfect three-sided pyramid

$$A(d) = 3\sqrt{3}d^2 \tan^2 \alpha, \quad (1)$$

where α is the angle at the apex of the AFM tip, defined as the angle of inclination of each of the three faces to the tip axis; or a sphere,

$$A(d) = \pi d(2R - d), \quad (2)$$

where R is the sphere radius. Since the real tip geometry is not axisymmetric, the tip radius derived with Eq. (2) is an average value over all directions.

III. RESULTS AND DISCUSSION

The hardness was first measured by imaging the residual indent with the indenter (diamond-coated tip). Three indents were made by applying maximum loads of 13.3, 13.8, and 16.5 μN on the gold single crystal. The maximum indent depths recorded on the force-depth curves were 9, 54, and 66 nm, respectively. Each residual indent was imaged by the indenter in tapping mode immediately after the indentation and later by a new and sharp silicon tip in contact mode. The shallow indent made at 13.3 μN could only be imaged with the sharp tip in the contact mode. All AFM images of the three indents scanned with the indenter or the sharp silicon tip show the same triangular indent shape that is similar to the expected cross-section of a three-sided pyramidal tip (Fig. 2). The residual indent depths measured with AFM images are smaller than the maximum depth measured on the force-depth curve. For example, for the indent at 13.8 μN, the depth of the residual indent measured with the AFM images is 21 nm for the blunt indenter [Fig. 2(a)] and 23 nm for the sharp tip [Fig. 2(b)]. These residual indent depths are significantly smaller than the maximum depth of 54 nm measured on the force-depth curve. The high slope of the unloading curve suggests that the elastic recovery is limited to below 10 nm. A small nonuniform elastic recovery can still significantly affect the measured residual indent depth due to the convolution of the tip and indent shapes.

More importantly, the area of the residual indent is systematically larger on the images collected with the sharp silicon tip than the ones collected with the indenter. As an example, for the indent at 13.8 μN, the residual indent area measured with the sharp tip (24.3×10^3 nm^2) is about three times larger than the area measured with the blunt indenter (7.6×10^3 nm^2). Similar observations were made on the indent made at 16.5 μN. The area of the residual indent measured on the AFM images scanned with the sharp tip is nearly four times larger than on those collected with the indenter. The larger residual indent area for the sharp tip cannot be explained by the deformation of the gold crystal during the AFM scanning in contact mode since the small set point of 3 nN used is negligible compared to the load required to deform the gold crystal plastically. The discrepancy in measured residual indent area is attributed to the convolution of the tip and the indent shapes.

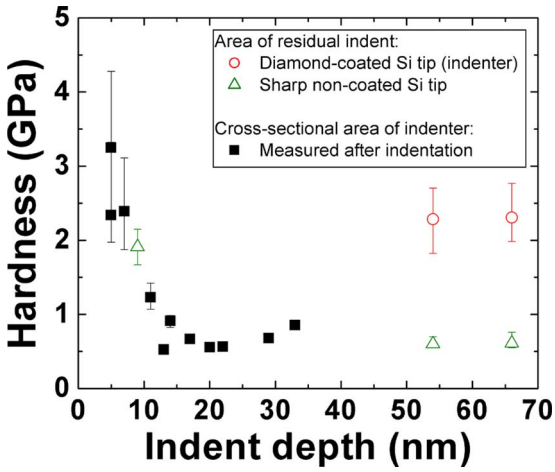

FIG. 3. (Color online) Comparison between the hardness values obtained by measuring the area of the residual indent from AFM images collected with the indenter (open circles) and a sharp Si tip (open triangles) and by measuring the cross-sectional area of the indenter after the indentation (solid squares).

The hardness measured at indent depths of 54 and 66 nm shows no significant depth dependence. The values were 0.60 and 0.61 GPa, respectively, when the area of the residual indent was estimated from images scanned with the sharp tip and 2.28 and 2.31 GPa, respectively, when scanned with the indenter (Fig. 3). The larger radius of the indenter leads to the systematic underestimation of the area and depth of the residual indent, and therefore an overestimation of the hardness. The indentation at a maximum depth of 9 nm yields a higher hardness value of 1.91 GPa. The error bars give the range of hardness values obtained from images of the residual indent scanned at different scanning rates, directions, and set points. These results suggest a depth dependence of the hardness only for depths smaller than 50 nm. This depth dependence was previously found in thin gold films and single crystals.[22,23,30] However, indenting the sample with a diamond-coated tip and then imaging the residual indent with a sharp tip are impractical for indent depths at the nanoscale. The method requires elaborate alignment marks to return to the same indent after a tip change. Also, the measurement of the area of the residual indent can be complicated by the uncertain amount of pileup around the indent that should be included. Pileups affect the depth along which the indenter and the sample are in contact and generally lead to the underestimation of the contact area.[31] These technical challenges motivate the development of a method

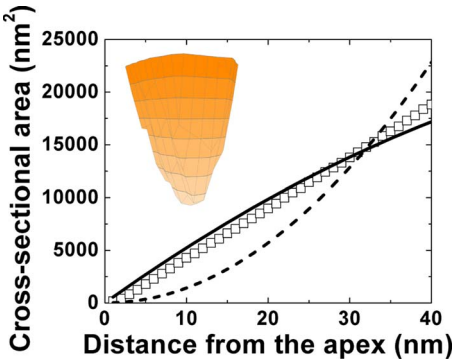

FIG. 4. (Color online) Typical area function of the indenter (open squares) measured with AFM images (inset). The data were fitted by modeling the tip as a sphere (solid line) or a perfect three-sided pyramid (dashed line).

to measure the hardness without imaging the residual indent or without calibration to a different standard.

The proposed method is based on the determination of the cross-sectional area of the indenter as a function of the distance from the apex. The hardness is then defined as the ratio between the maximum load and the cross-sectional area of the indenter at maximum indent depth. The tip shape can be determined by scanning a silicon grating TGT01, so no alignment marks or tip change is required, saving a considerable amount of time. Also, the tip shape can be monitored before and after each indent. For this method, the indent depth was limited to depths below 40 nm in order to limit the effect of pileups. The scanner velocity in the normal direction was intentionally kept constant at 0.6 μm/s. Hardness values measured with scanner velocities between 0.5 and 0.8 μm/s showed no significant difference over the same depth range (data not shown).

Using this method, two series of hardness values were obtained using two different tips as indenters: a diamond-coated silicon tip and a sharper noncoated silicon tip. The area function (cross-sectional area of the tip as a function of the distance from the apex) measured with AFM images is typically almost linear for distances below 40 nm, characteristic of an imperfect paraboloid tip (Fig. 4). A comparison between the fits using a perfect three-sided pyramid model [Eq. (1)] or a sphere model [Eq. (2)] reveals that a sphere model describes the tip shape better over this distance range. These fits provide an average value of the tip radius of 70 ± 12 nm for the noncoated silicon tip and 112 ± 26 nm for the diamond-coated tip. The error reflects the range of values obtained over the entire series of nanoindentations.

Images of the tip before and after each indent reveal that the tip radius can vary by almost 20 nm after one indentation test. The average difference between the radii before and after the indent is 11 nm for the noncoated silicon tip and 15 nm for the diamond-coated tip. These relatively large variations of the tip radius actually reflect the nonspherical tip shape rather than a significant modification in the area function. Discrepancies between the hardness values obtained using the area function before and after the indent exceed the error bars only for the noncoated tip and for indent depths below 15 nm [Fig. 5(a)]. The errors on the hardness values are related mainly to the uncertainty on the cross-sectional

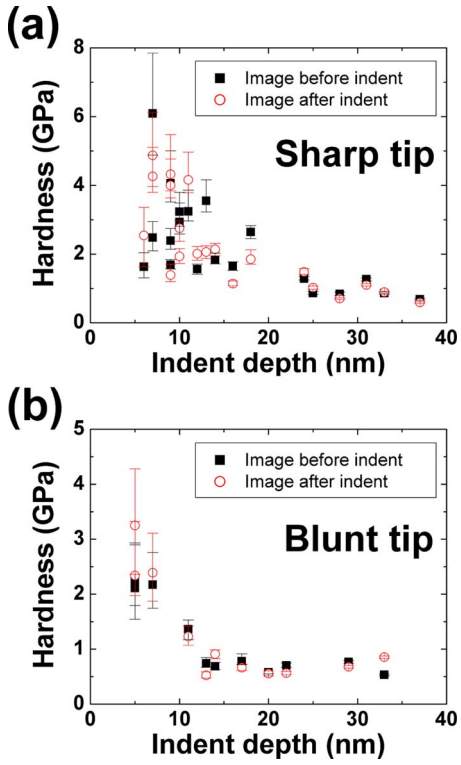

FIG. 5. (Color online) Hardness as a function of the indentation depth. Comparison between the hardness values determined using images of the indenter before and after the indent for (a) a sharp tip and (b) a blunt tip.

area. The error bars reflect the range of cross-sectional areas estimated at distances from the apex within 1 nm from the maximum indent depth.

Data from both measurement techniques show a depth dependence on hardness for depths smaller than 25 nm. The hardness decreases as the depth increases from 5 to 20 nm and then remains constant for depths larger than 30 nm (Fig. 5). This depth dependence of the hardness cannot be attributed to a substrate effect since the indent depth range is very small compared to the thickness of 2 mm of the gold crystal. The hardness values obtained with the diamond-coated tip using the images after indent [Fig. 5(b)] also match those obtained from AFM images of the residual indent scanned with the sharp tip (Fig. 2). The hardness values obtained with images of the indenter are between 0.6 and 0.8 GPa for depths larger than 20 nm, consistent with the 0.6 GPa value obtained with images of the residual indent at depths above 50 nm. The 1.91 GPa value for the 9 nm deep indent, measured from AFM images of the residual indent, also follows the trend suggested by the data from the cross-sectional area of the indenter.

Finally, the two series of hardness data obtained with the two tips using images of the indenter after indent are compared to study the effect of tip radius on the measured hardness (Fig. 6). The hardness values obtained using the sharp indenter are systematically higher than those using the blunt indenter for depths smaller than 30 nm. For depths larger than 30 nm, the hardness values are close to 0.6 GPa for both series of data. The lower hardness values for the blunt tip cannot be explained only by the diamond coating: the presence of the diamond coating is expected to increase the re-

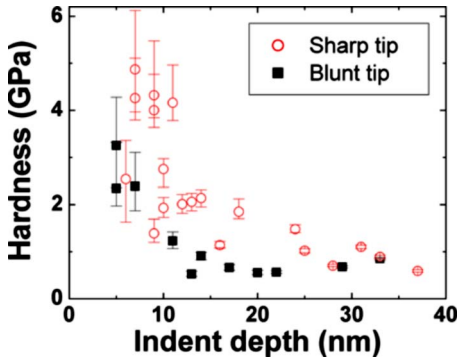

FIG. 6. (Color online) Comparison between the hardness values obtained using a sharp tip (open circles) or a blunt tip (solid squares) as the indenter. The data were determined using the images of the indenter after the indent.

duced modulus of the tip-sample contact and lead to lower hardness values over the entire depth range. The similar values obtained at depths larger than 30 nm indicate that the diamond coating has a very limited effect on the hardness measurements.

The hardness values reach a constant value for depths above 15 nm for the blunt tip and above 30 nm for the sharp tip. For spherical and rounded nonspherical indenters, the depth range over which the hardness depth dependence is the most pronounced should be of the order of the tip radius.[14] Therefore, a smaller tip radius should result in a narrower depth range over which the hardness is depth dependent. The experimental contact radius can be estimated by the radius of the equivalent circle of contact delimiting the cross-sectional area of the indenter at maximum indent depth. When the hardness data in Fig. 6 are plotted against the ratio between contact radius a and tip radius R or against the d/R ratio[14] (data not shown), the indentation size effect is still observed over a wider range of a/R or d/R with the sharp tip than with the blunt tip ($a/R<0.8$ with the sharp tip instead of $a/R<0.5$ with the blunt tip, and $d/R<0.15$ with the sharp tip instead of $d/R<0.3$ with the blunt tip). The data indicate an inherent difference in obtaining data from tips with different shapes even when attempting to account for differences in the projected indent area. This effect may be driven by a difference in the gradient of deformation outside the sharp tip and the need for more geometrically necessary dislocations.

IV. CONCLUSIONS

The effect of tip radius on AFM nanoindentation was investigated through indentation on the (111) face of a gold single crystal. The hardness was derived using two different methods: measuring directly the projected area of the residual indent with AFM images and measuring the cross-sectional area of the indenter before and after each nanoindentation test. The hardness values obtained from the cross-sectional area of the indenter are comparable with those obtained from images of the residual indent scanned with a sharp tip. Two AFM tips of average radii of 70 ± 12 and 112 ± 26 nm were used to indent the sample to various depths ranging from 4 to 50 nm. For depths above 30 nm, hardness values remain constant around 500 MPa for both indenters. For depths below 30 nm, the hardness increases as the indent depth decreases for the sharp and blunt indenters, and this indent depth dependence is observed over a wider depth range for the sharp indenter. For depths below 30 nm, the hardness values obtained with the sharp indenter are also consistently higher than those obtained with the blunt indenter. The results confirm a size scale effect during nanometer scale indentation for both varying penetration depth and tip radius, both of which influence the volume of material sampled during deformation.

ACKNOWLEDGMENTS

The authors acknowledge the financial support from the Department of Energy under Grant No. DE-FG02-06ER46293.

[1]W. C. Oliver and G. M. Pharr, J. Mater. Res. **19**, 3 (2004).
[2]Y.-T. Cheng and C.-M. Cheng, Mater. Sci. Eng., R. **44**, 91 (2004).
[3]W. C. Oliver and G. M. Pharr, J. Mater. Res. **7**, 1564 (1992).
[4]M. F. Doerner and W. D. Nix, J. Mater. Res. **1**, 601 (1986).
[5]I. N. Sneddon, Int. J. Eng. Sci. **3**, 47 (1965).
[6]K. W. McElhaney, J. J. Vlassak, and W. D. Nix, J. Mater. Res. **13**, 1300 (1998).
[7]J. H. Strader, S. Shim, H. Bei, W. C. Oliver, and G. M. Pharr, Philos. Mag. **86**, 5285 (2006).
[8]J. M. Meza, F. Abbes, and M. Troyon, J. Mater. Res. **23**, 725 (2008).
[9]K. Ikezawa and T. Maruyama, J. Appl. Phys. **91**, 9689 (2002).
[10]F. M. Borodich, L. M. Keer, and C. S. Korach, Nanotechnology **14**, 803 (2003).
[11]H. Bei, E. P. George, J. L. Hay, and G. M. Pharr, Phys. Rev. Lett. **95**, 045501 (2005).
[12]S. Qu, Y. Huang, W. D. Nix, H. Jiang, F. Zhang, and K. C. Hwang, J. Mater. Res. **19**, 3423 (2004).
[13]C.-J. Lu and D. B. Bogy, Int. J. Solids Struct. **32**, 1759 (1995).
[14]W. Chen, M. Li, T. Zhang, Y.-T. Cheng, and C.-M. Cheng, Mater. Sci. Eng., A **445–446**, 323 (2007).
[15]N. Yu, A. A. Polycarpou, and T. F. Conry, Thin Solid Films **450**, 295 (2004).
[16]A. J. Bushby and D. J. Dunstan, J. Mater. Res. **19**, 137 (2004).
[17]I. J. Spary, A. J. Bushby, and N. M. Jennett, Philos. Mag. **86**, 5581 (2006).
[18]L. Calabri, N. Pugno, A. Rota, D. Marchetto, and S. Valeri, J. Phys.: Condens. Matter **19**, 395002 (2007).
[19]J. G. Swadener, E. P. George, and G. M. Pharr, J. Mech. Phys. Solids **50**, 681 (2002).
[20]A. Widjaja, A. Needleman, and E. Van der Giessen, Modell. Simul. Mater. Sci. Eng. **15**, S121 (2007).
[21]Y. Huang, F. Zhang, K. C. Hwang, W. D. Nix, G. M. Pharr, and G. Feng, J. Mech. Phys. Solids **54**, 1668 (2006).
[22]M. J. Cordill, D. M. Hallman, N. R. Moody, D. P. Adams, and W. W. Gerberich, Metall. Mater. Trans. A **38**, 2154 (2007).
[23]M. Göken, M. Kempf, M. Bordenet, and H. Vehoff, Surf. Interface Anal. **27**, 302 (1999).
[24]R. Saha and W. D. Nix, Acta Mater. **50**, 23 (2002).
[25]W. D. Nix and H. Gao, J. Mech. Phys. Solids **46**, 411 (1998).
[26]D. Tabor, *Hardness of Metals* (Clarendon, Oxford, 1951).
[27]M. R. VanLandingham, T. F. Juliano, and M. J. Hagon, Meas. Sci. Technol. **16**, 2173 (2005).
[28]J. E. Sader, J. W. M. Chon, and P. Mulvaney, Rev. Sci. Instrum. **70**, 3967 (1999).
[29]J. S. Villarrubia, J. Res. Natl. Inst. Stand. Technol. **102**, 425 (1997).
[30]S. G. Corcoran, R. J. Colton, E. T. Lilleodden, and W. W. Gerberich, Phys. Rev. B **55**, R16057 (1997).
[31]A. Bolshakov and G. M. Pharr, J. Mater. Res. **13**, 1049 (1998).